Chinese Journal of Aeronautics, 2013,26(1): 217–223

Chinese Society of Aeronautics and Astronautics
& Beihang University

Chinese Journal of Aeronautics

cja@buaa.edu.cn
www.sciencedirect.com

Research on modeling of heat source for electron beam welding fusion-solidification zone

Wang Yajun [a,*], Fu Pengfei [b], Guan Yongjun [c], Lu Zhijun [b], Wei Yintao [d]

[a] *School of Mechanical Engineering and Automation, Beihang University, Beijing 100191, China*
[b] *Science and Technology on Power Beam Processes Laboratory, Beijing Aeronautical Manufacturing Technology Research Institute, Beijing 100024, China*
[c] *State Key Laboratory of Nonlinear Mechanics, Institute of Mechanics, Chinese Academy of Sciences, Beijing 100190, China*
[d] *State Key Laboratory of Automotive Safety and Energy, Department of Automotive Engineering, Tsinghua University, Beijing 100084, China*

Received 16 October 2011; revised 16 December 2011; accepted 7 October 2012
Available online 16 January 2013

KEYWORDS

Electron beam welding (EBW);
Fusion-solidification zone;
Heat source model;
Temperature fields;
Weld shape

Abstract In this paper, the common heat source model of point and linear heat source in the numerical simulation of electron beam welding (EBW) were summarized and introduced. The combined point-linear heat source model was brought forward and to simulate the welding temperature fields of EBW and predicting the weld shape. The model parameters were put forward and regulated in the combined model, which included the ratio of point heat source to linear heat source Q_{pr} and the distribution of linear heat source L_r. Based on the combined model, the welding temperature fields of EBW were investigated. The results show that the predicted weld shapes are conformable to those of the actual, the temperature fields are reasonable and correct by simulating with combined point-linear heat source model and the typical weld shapes are gained.

1. Introduction

Electron beam welding (EBW) is widely employed in many fields because of high depth–width ratios obtainable. An electron beam is precisely regulated to deflect and focus, which leads to a high-power density. When the beam irradiates on a work-piece, the metal of the work-piece rapidly melts and vaporizes, resulting in a deep and narrow keyhole surrounded by fusion-solidification zone. As the beam passes along the work-piece, the molten metal quickly fills in the vaporized hole and solidifies. The main advantages of this technology lie in big depth–width ratios, defects free, small heat-affected zone and high efficiency. Therefore, EBW is an important technology in the high-precise and high-quality manufacturing field.[1–8]

EBW is a complicated and dynamic phase in high temperature and is influenced by the welding parameters, the thermal material properties and the beam characteristics, which include the beam power, energy density distribution, welding speed, focal location and spot size. The real-time measurements through the experiments are difficult and the numerical simulation of EBW was an effective research method[1] to realize the welding principle, even to improve welding quality.

* Corresponding author. Tel.: +86 10 62496020.
E-mail address: wangyj625@sina.com (Y. Wang).

Peer review under responsibility of Editorial Committee of CJA.

Production and hosting by Elsevier

1000-9361 © 2013 CSAA & BUAA. Production and hosting by Elsevier Ltd. Open access under CC BY-NC-ND license.
http://dx.doi.org/10.1016/j.cja.2012.12.023

Because of the high-power density, the keyhole effect accompanied with EBW leads to high depth–width ratio of the weld, which results in the typical weld with nail shape. For the particular energy distribution, Wu and Zhao[9] put forward the rotary Gaussian-distributed heat sources model and got precise simulation results. To reduce the errors of the weld geometry shape, the suitable heat source model is essential for different welding and different weld depths.

Klykow et al.[10] brought forward the column heat source model related to keyhole effect and energy transfer, and the surface heat source model represents the radiation. Both sources had a Gaussian power distribution. During laser welding, the plasma was an independent heat source on the surface and laser beam welding with a column source results in a dagger shape form of the penetration zone.

Steen et al.[11] combined the Rosenthal point and linear source and put forward a new heat source model, which was effective to simulate the welding keyhole and estimate the power during welding. The linear source represents the absorption of the keyhole, and the point source expresses the plasma radiation. The results show that the width of the weld is proportional to the energy density of the linear source.

Swift-Hook and Gick[12] supposed that the energy was absorbed by the workpiece and used the simplified line source heat model to calculate the shapes of electron beam welds. However, the line-source model has some defects. First, the infinite temperature field occurs near the sources; second, the distribution of incident flux is not considered.

Ziolrowski and Brauere[13] brought forward a volumetric heat source and modeled the seebeck effect and temperature distribution. The heat source presented a 3D model of deep welding of different metals and modeled electron beam deflection resulting from the thermoelectric fields caused by seebeck effect.

Ho et al.[14] brought forward an analytical model assuming a paraboloid of revolution for the keyhole and predicted the temperature in the keyhole. Considering the momentum balance at the bottom of the keyhole, the analytical solution based on the model predicted that the temperature distribution is more consistent with the experimental data.

Guo et al.[15] put forward a Gaussian heat source model from the joint micrographic and temperature measurements. The heat source composed of two parts. One part with most power was used to create the keyhole inside the materials and the other part with a ring shape was a surface heat source neglected in the investigation. The simulation with these distributions predicted the fused and HAZ zone close enough to the experimental joint shape.

Ferro et al.[16] proposed a superimposition of a spherical and a conical shape heat source (two volumetric heat sources) with Gaussian distribution for the EBW of Inconel706. The shape of the fusion zone was simulated with a reasonable degree of accuracy, which improved the correct thermal and residual stresses prediction.

Rai et al.[17] put forward an energy balance model considering the variation keyhole wall and calculated the fluid flow and heat transfer during EBW. The investigation presented the simulation results of temperature fields, thermal cycles, weld geometry and fluid flow.

The researches of the thermal simulation for the welding were investigated with the single surface heat source or volumetric heat source, and the weld pool shape simulated from the single heat source represents the shape errors from the weld. About high-power density and keyhole effect for titanium alloy with EBW, the combined point-linear heat source model employed in the investigation is essential to predict weld shape and keep the coincidence with the weld geometry shape.

Heat transfer and fluid flow during electron beam welding have been recently investigated by the fluid model, which are optimal to model the keyhole. But the numerical models were complex, only the keyhole shape is assumed to be a revolute paraboloid model and the validation of the model is difficult.

In the paper, the common heat source model of point and linear heat source are summarized and introduced in the numerical simulation of EBW. The combined point-linear heat source model is put forward and applied to predicting the weld shape in EBW. The paper has great significance for theoretical study of electron beam welding.

2. Heat source model of EBW

2.1. Restraining equation

According to the principle of electron beam welding, the point-linear heat source model is put forward (see Fig. 1).

The expression of the point heat source[11] is as follows:

$$-v_b \frac{\partial T}{\partial x} = \frac{\lambda}{c\rho}\Delta T + \frac{1}{c\rho} q(x, y, z) \tag{1}$$

where v_b is welding speed, λ the thermal coefficient, ρ density of the base metal, c specific heat, and q heat source of the volume.

The boundary of surface heat flow and the heat input q (x, y, z) are calculated with the acceleration voltage U_a, beam current I_a, focusing current I_f and environmental factor. The weld width and sample thickness of the work-piece are included in the boundary condition.

According to Eq. (1), the isolines of the melting temperature are calculated and ascertained and the weld shape could be obtained. The melting part ($T \geqslant T_m$) is defined as the fusion–solidification zone in the paper.

2.2. Heat source model

Based on the keyhole effect on the surface, the energy of point heat source Q_p is the surface heat input in Fig. 1. The energy of linear heat source Q_l is the heat input of linear body column, which is the keyhole effect.

Obviously, the energy of the point heat source and linear heat source are

$$Q_p + Q_l = \eta P = \mu U_a I_b \tag{2}$$

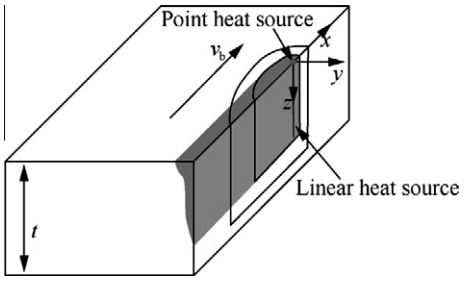

Fig. 1 Heat source model.

The ratios of Q_p and Q_l are regulated during the experiment and η is the coefficient of effective power.

The energy distribution of linear heat source power is expressed as

$$q(z) = \frac{Q_l}{H} \tag{3}$$

However, the energy density distribution of heat source along the weld depth (H) is not equal and L_r is defined to denote the unsymmetrical:

$$L_r = \frac{q(H)}{q(0)} \tag{4}$$

The symbol of $q(0)$ is the energy of linear heat source on the surface ($z = 0$), and $q(H)$ the energy of linear heat source in the depth ($z = H$).

$$0 \leqslant L_r \leqslant 1 \tag{5}$$

When $L_r = 1$, the distribution of linear source is symmetrical; when $L_r = 0$, the distribution of linear source is attenuated, and the power density of linear heat source in the depth ($z = H$) is zero.

In general, the distribution of linear heat source is given as

$$q(z) = f(z) \tag{6}$$

The symbol of $q(z)$ is linear power density of linear heat source, where the maximum distance from the surface is z and $q(z)$ is met:

$$\int_0^H q(z)d(z) = Q_l \tag{7}$$

The above heat source models are the heat input for the temperature calculation, which is important to simulate welding temperature field.

3. Temperature field of EBW

Suppose a point heat source Q is located at the moving coordinates (x, y, z_0) and the temperature field of moving point heat source in the infinite body is given for the sheet:

$$\widetilde{T}(x, R_1, z - z_0, z_0) = \frac{Q}{4\pi\lambda R} e^{-v_b\left(\frac{x+\sqrt{R_1^2+(z-z_0)^2}}{2\alpha}\right)} \tag{8}$$

where z_0 is the coordinate of the point heat source, α thermal diffusion coefficient, R_1 the distance from the coordinate (x, y) to the origin of coordinate (0,0), R the distance from the coordinate (x, y, z) to origin of coordinate (0,0,z_0),

$$R_1^2 = x^2 + y^2, \quad R^2 = x^2 + y^2 + (z - z_0)^2$$

When the thickness of the workpiece is t, the temperature in the infinite body shown in Eq. (8) should be modified. With regard to the periodic boundary condition, the corresponding temperature field is obtained:

$$\begin{aligned}
T_{Q_p}(v_b, x, R_1, z - z_0, z_0) &= \widetilde{T}_{Q_p}(v_b, x, R_1, z - z_0, z_0) + \widetilde{T}_{Q_p}(v_b, x, R_1, z + z_0, z_0) \\
&+ \sum_{i=1}^{\infty}[\widetilde{T}_{Q_p}(v_b, x, R_1, 2i \cdot t - z - z_0, z_0) + \widetilde{T}_{Q_p}(v_b, x, R_1, 2i \cdot t + z - z_0, z_0) \\
&+ \widetilde{T}_{Q_p}(v_b, x, R_1, 2i \cdot t - z + z_0, z_0) + \widetilde{T}_{Q_p}(v_b, x, R_1, 2i \cdot t + z + z_0, z_0)] \\
&= \frac{Q}{4\pi\lambda R} e^{-\frac{v_b \cdot x}{2\alpha}} \overline{T}_{Q_p}(v_b, z_0, x, y, z)
\end{aligned} \tag{9}$$

where

$$\begin{aligned}
\overline{T}_{Q_p}(v_b, z_0, x, y, z) &= e^{\frac{-v_b\sqrt{R_1^2+(z-z_0)^2}}{2\alpha}} + e^{\frac{-v_b\sqrt{R_1^2+(z+z_0)^2}}{2\alpha}} \\
&+ \sum_{i=1}^{\infty}\left(e^{\frac{-v_b\sqrt{R_1^2+(2i\cdot t-z-z_0)^2}}{2\alpha}} + e^{\frac{-v_b\sqrt{R_1^2+(2i\cdot t+z-z_0)^2}}{2\alpha}} + e^{\frac{-v_b\sqrt{R_1^2+(2i\cdot t-z+z_0)^2}}{2\alpha}} + e^{\frac{-v_b\sqrt{R_1^2+(2i\cdot t+z+z_0)^2}}{2\alpha}}\right)
\end{aligned} \tag{10}$$

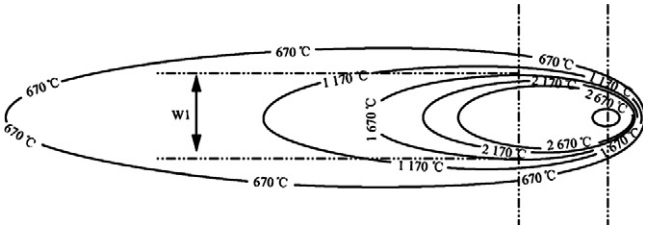

Fig. 2 Zone of the maximum temperature distribution in EBW.

When welding speed v_b and the depth of heat source z_0 are known, the distribution of $\overline{T}$ in the space could be attained from the summation of the series.

For the linear heat source in the finite depth body, the infinitesimal $q\mathrm{d}z_0$ is taken as point heat source, then

$$T_{q\mathrm{d}z_0}(x, R_1, z - z_0, z_0) = \frac{q\mathrm{d}z_0}{4\pi\lambda R} \mathrm{e}^{-\frac{v_b \cdot x}{2a}} \overline{T}_{Q_p}(v_b, x, R_1, z, z_0) \tag{11}$$

The temperature field produced by the linear heat source is obtained by integrating $q\mathrm{d}z_0$ along the linear heat source:

$$T_{Q_l} = \frac{\mathrm{e}^{-\frac{v_b \cdot x}{2a}}}{4\pi\lambda R} \int_0^H \overline{T}_{Q_p}(v_b, x, R_1, z, z_0) q\mathrm{d}z_0 \tag{12}$$

According to the superposition principle, the temperature field produced by linear heat source and point heat source is

$$T = T_{Q_l} + T_{Q_p} \tag{13}$$

The temperature field in Eq. (13) is a quasi-steady temperature field, which is in the moving coordinate. Each point in the workpiece has a temperature history of the rising and falling phases. The external temperature distribution in EBW is shown in Fig. 2.

By drawing a series of the beelines along the welding direction, the temperature is simulated on the beeline and is projected on the plane of (y, z), which ranges from 670 to 2670 °C. Then the maximum temperature distribution in the section is gained, which is vertical in the EBW direction. In the plane, the region reaching the temperature of the melting point is fusion–solidification zone (marked by W1 in Fig. 2). The heating energy of the material phase change is ignored in the model and the overestimation of the weld shape is in the simulation based on the value of T_m. To avoid the errors, the critical temperature of T'_m is put forward to substitute T_m.

$$T > T_m \tag{14}$$

It is assumed that the melting latent heat of the material is ΔH and the heat input in a unit mass is Q. When ignoring the melting latent heat, the temperature is given as follows:

$$T = T_0 + \Delta T = T_0 + \frac{Q}{c} \tag{15}$$

where c is the specific heat. If $T = T_0 + \Delta T > T_m$, the temperature is

$$T' = T_0 + \frac{Q}{c} - \frac{\Delta H}{c} = T - \frac{\Delta H}{c} \tag{16}$$

where $T_0 + \frac{Q}{c} - \frac{\Delta H}{c} > T_m$.

Considering Eq. (16) and the temperature calculated from Eq. (13), the boundary of the fusion–solidification zone is calculated by the substitution of T'_m for T_m.

$$T'_m = T_m + \frac{\Delta H}{c} \tag{17}$$

where T'_m is higher than T_m by 173 °C for titanium alloy.

The parameters of heat source model are described for titanium alloy with EBW in Table 1, in which the temperature field for EBW is calculated.

4. Simulation results and discussion

4.1. Temperature fields and weld shapes

The temperature field and weld shape with EBW were calculated and simulated by the combined heat source model of TC4 titanium alloy with the thickness of 20 mm. Because of

Table 1 Parameters of heat model for welding temperature field.

Symbol	Signification	Unit	Explanation
Q	Total power, influenced by acceleration voltage and electron beam current	W	$U_a \cdot I_b$
H	Weld depth	m	
η	Heat efficiency of welding		Range:70%–90%
Q_p,Q_l	Energy of the point and linear heat source	W	Influenced by the location of the focal point
L_r	Coefficient of energy distribution of linear heat source		The proportion of the heat source in the maximum depth and on the surface
Q_{pr}	Ratio of the point heat source energy (Q_p) to the total energy (Q). The ratio of the energy (Q_l) is ($1-Q_{Pr}$)		0–1
λ	Heat conductivity	$W \cdot m^{-1} \cdot K^{-1}$	
ρ	Density	$kg \cdot m^{-3}$	
c	Specific heat	$J \cdot kg^{-1} \cdot K^{-1}$	
T_m	Melting point	K	
ΔH	Melting latent heat	$J \cdot kg^{-1}$	Adjust the critical temperature when determining the boundary of the weld. The value is 92 kJ/kg for the titanium alloy
v_b	Welding speed	$m \cdot s^{-1}$	
t	Depth of workpiece	m	

Table 2 Parameters in the calculating model.

No.	T_m (°C)	λ (W·m^{-1}·K^{-1})	ρ (kg·m^{-3})	c (J·kg^{-1}·K^{-1})	Q (W)	v (m·s^{-1})	t (m)	η (%)	H (m)	L_r
1	1670	7.0	4500	530	4392	0.01	0.02	90	0.01	1
2	1670	7.0	4500	530	4392	0.01	0.02	90	0.01	0

the aberration temperature during the modeling by the linear heat source, the temperatures were substituted for the boiling point temperature, which were higher than that of the boiling point during the simulation. The parameters were used for the modeling in Table 2. The ratio of the energy Q_p to the total energy Q was defined as Q_{pr}, which was the energy ratio of point heat source to linear heat source. With the Q_{pr} parts of 0, 0.05, 0.3 and 0.4, the distributions of the temperature field were obtained. The temperature of solidification boundary with no latent heat was 1670 °C, the temperature with the latent heat was 1873 °C, and the zone of solidification boundary represented the weld shapes.

When the distributions of linear heat source were even, the temperature distributions and weld shape by modeling are shown in Fig. 3, and a series of different weld shapes with different Q_{pr} parts was calculated and obtained. When the linear heat source attenuated to zero, the temperature distributions are in Fig. 4, and the shape prediction of the weld toe with the attenuating linear heat source were almost coincident with that of the welds.

4.2. Validation

The optimum parameters of Q_{pr}, L_r and η are 0.1%, 1% and 90%, which were optimized by a lot of simulation. In different welding processes (in Table 3), different weld shapes are gained by the modeling and the metallographic tests, which include funnel pattern, chock pattern, bell pattern and nail pattern (see Fig. 5). In the simulation, the depth of the linear heat source is equal to weld depth, and the energy distribution coefficient of linear heat source L_r is 1 with the weld efficiency of 90%. Comparison between the actual weld and the predicted weld is shown in Fig. 5. The actual weld shapes are almost identical with those of the predicted results and the heat source model was optimal to EBW.

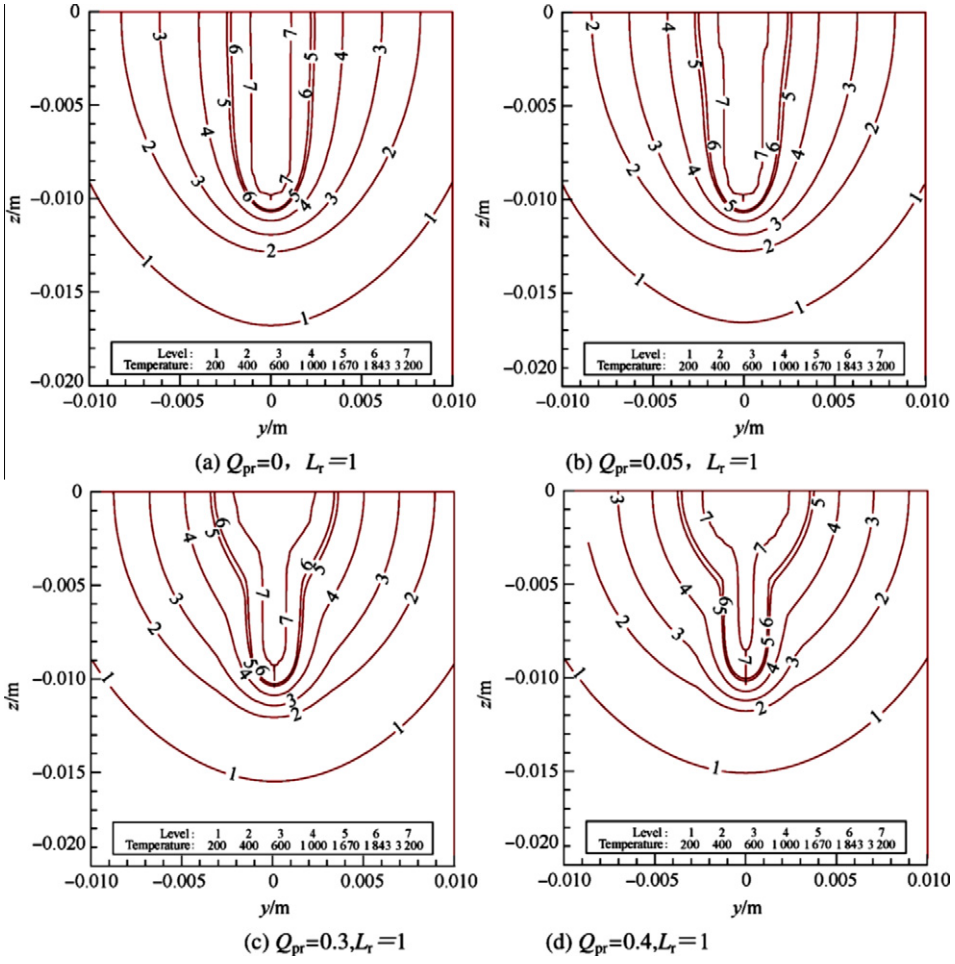

Fig. 3 Distribution of temperature in weld section.

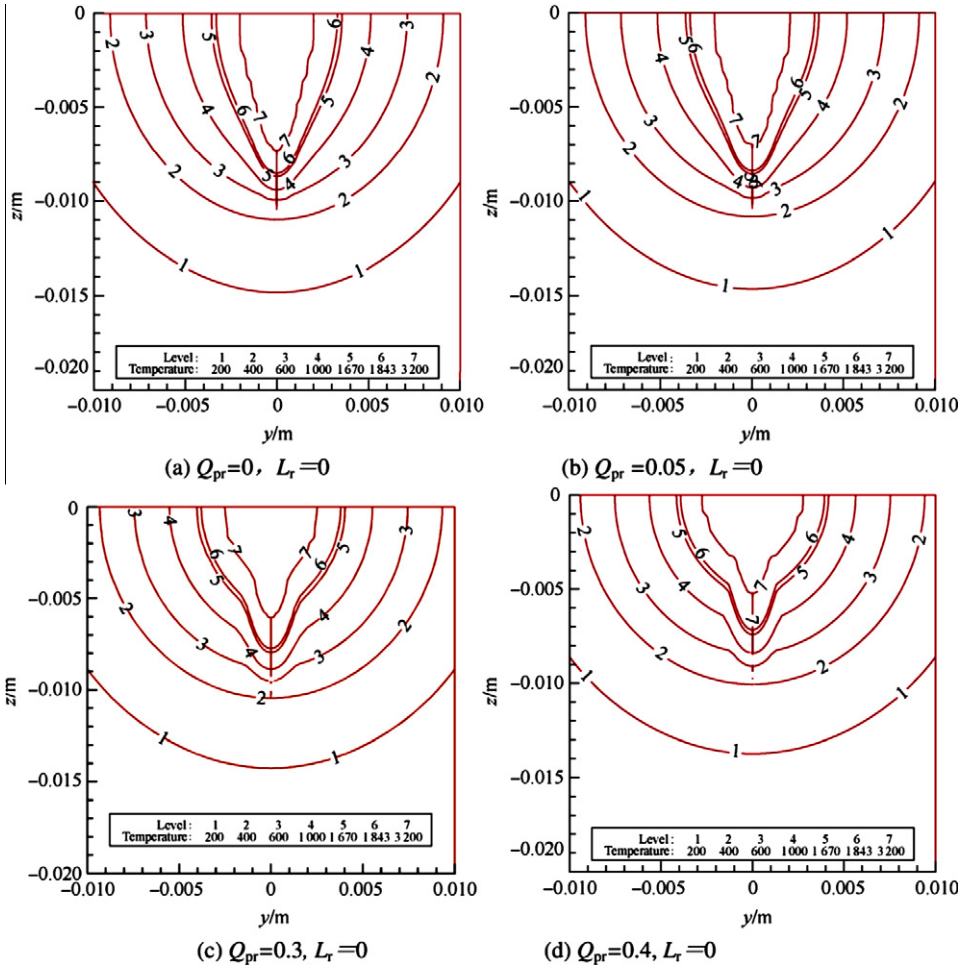

Fig. 4 Distribution of temperature in weld section.

Table 3 Process and calculation parameters.

Acceleration voltage U_a (kV)	Weld speed V (mm·min^{-1})	Focused current I_f (mA)	Beam current I_b (mA)	Weld depth H (mm)	Ratio of point heat source Q_{pr}	Weld shape
90	600	1680	48.8	16	0.3	Funnel
90	300	1681	51.1	20	0.15	Chock
90	300	1650	40.5	18	0.05	Bell
150	800	2220	25.5	16	0.1	Nail

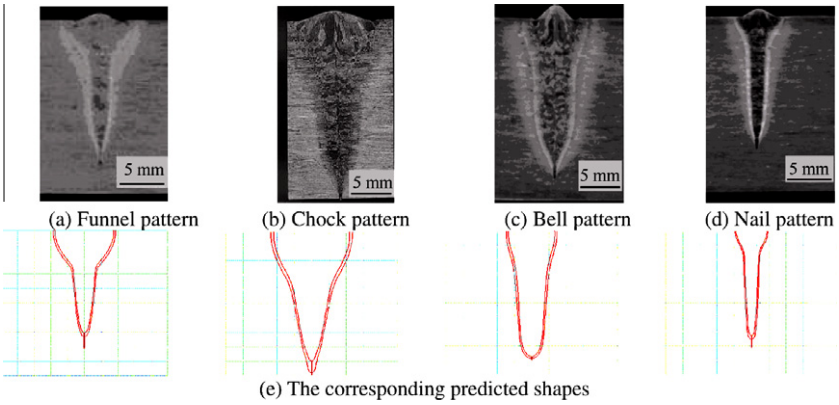

Fig. 5 Comparison of weld shape and predicted weld shape.

The heat source models and the parameters are essential to simulate the welding temperature of EBW, which correctly predict the weld shape.

With the adjustment of the acceleration voltage U_a and beam current I_a, the welding energy Q could be altered in heat source model. And the parameters of Q_{pr} and L_r are regulated by the focusing current I_f. Therefore, welding temperature fields of the simulation are optimized by the optimum parameters of heat source and welding speeds.

With the reduction of Q_{pr} and the increase of L_r, the weld shapes by modeling are more conformable with those of the actual weld, whose computation results are also in agreement with experimental data of Refs.[18–20], and the welding temperature fields of EBW are reasonable by simulating with the models.

The relationship of weld shape and process parameters would be acquired by the experiment and simulation, which would contribute to optimizing the EBW process, lessening the costing and shortening production period.

5. Conclusions

(1) The combined point-linear model is put forward and the relevant formula is deduced for welding temperature, which are investigated on the simulation of EBW temperature fields for titanium alloy. The value of Q_{pr} and energy distribution coefficient of linear heat source L_r have a significant influence on the weld shape.
(2) With the heat source model, the weld shapes predicted from temperature fields are conformable to those of the actual weld, and four weld shapes are gained including nail pattern, bell pattern, funnel pattern and chock pattern.

Acknowledgements

We would like to thank the anonymous reviewers for their critical and constructive review of the manuscript. This study was co-supported by the National Basic Research Program (No. 61362), the National Natural Science Foundation of China (No. 50935008 and 10902113), and Science Foundation of Aeronautics (No. 2010ZE25006).

References

1. Schultz H. *Electron beam welding*. 4th ed. Cambridge: Abington; 2003.
2. Robert W, Messler JR. The greatest story never told: EB welding on the F-14. *Weld J* 2007;**86**:41–7.
3. James DC, Larry, Henry RP. Titanium alloys on the F-22 fighter airframe. *Adv Mater Processes* 2002;**160**:25–8.
4. Mao ZY. Application analysis of electron beam welding technology in large aircraft. *Aeronaut Manuf Technol* 2009(2);92–4 Chinese.
5. Gong SL, Li HX, Li X. Application and development of high energy beam manufacturing technology. *Aeronaut Manuf Technol* 2009;34–7 [Chinese].
6. Henderson MB, Arrell D, Larsson R, Heobel M, Marchant G. Nickel based superalloy welding practices for industrial gas turbine applications. *Sci Technol Weld Join* 2004;**9**:13–21.
7. Li CX, He CD, Xu QJ, Jiang CY. Design of electrostatic focusing system of space electron beam. *Chin J Aeronaut* 2005;**18**:256–62.
8. Tan LJ, Yao ZK, Qin C, Guo HZ, Zhang JW. Effects of deformation temperature on microstructure and mechanical properties of electron beam welded joint of dissimilar titanium alloys. *Chin J Nonferrous Met* 2010;**20**:1533–8.
9. Wu S, Zhao HY, Wang Y, Zhang XH, et al. A new heat source model in numerical simulation of high energy beam welding. *Trans China Weld Inst* 2004;**25**:91–4, in [Chinese].
10. Klykow NA, Dammer AA, Druzhinin AV, Malysh MM. *Weld Int* 1987;**10**:914–6.
11. Steen WM, Dowden J, Davis M, Kapadia P. A point and line source model of laser keyhole welding. *J Phys D: Appl Phys* 1998;**21**:1255–60.
12. Swift-Hook DT, Gick AEF. Penetration welding with lasers. *Weld J* 1973;**52**:492–9.
13. Ziolrowski M, Brauere H. Modelling of seebeck effect in electron beam deep welding of dissimilar metals. *COMPEL: the international journal for computation and mathematics in electrical and electronic engineering* 2009;**28**(1):140–53.
14. Ho CY, Wen MY, Lee YC. Analytical solution for three-dimensional model predicting temperature in the welding cavity of electron beam. *Vacacuum* 2008;**82**(3):316–20.
15. Guo J, Le Masson P, Artioukhine E, Loulou T, Rogeon P, Carin M, et al. Estimation of a source term in a two-dimensional heat transfer problem: application to an electron beam welding. *Inverse Prob Sci Eng* 2006;**14**:21–38.
16. Ferro P, Zambon A, Bonollo F. Investigation of electron-beam welding in wrought Inconel706-experimental and numerical analysis. *Mater Sci Eng A* 2005;**392**:94–105.
17. Rai R, Elmer JW, Palmer TA, DebRoy T. Heat transfer and fluid flow during electron beam welding of 21 Gr–6Ni–9Mn steel and Ti–6Al–4V alloy. *J Phys D: Appl Phys* 2009;**42**:1–12.
18. Wang YJ, Guan YJ, Fu PF, Wei YT, Lu ZJ. Study on shape factor of the fusion-solidification zone of electron beam weld. *China Weld* 2008;**17**:62–7.
19. Fu PF, Wang YJ, Mao ZY, Gong SL, Wang CM. Study on character of electron beam dynamic focus during EBW. *J Aeronaut Mater* 2009;**29**:38–41 [Chinese].
20. Zhang WY. *Theory of welding heat transfer*. 1st ed. Beijing: Mechanical Industry Press; 1989 [Chinese].

Wang Yajun received the B.S. degree from Dalian Jiaotong University in 1985, and then worked in Beijing Aeronautical Manufacturing Technology Research Institute; she has worked in Beijing Aviation Material Institute since 2009. She is a doctorial candidate in Beihang university, her main research interest is the processing of Electron Beam Welding.